Leveraging Fluid Resistance in Soft Robots

Chaim C. Futran[1], Steven Ceron[1], Benjamin C. Mac Murray[2], Robert F. Shepherd[1], Kirstin H. Petersen[3]

***Abstract*— A key advantage to Fluidic Elastomer Actuators (FEA) is that they permit easy fabrication of robots capable of sophisticated manipulation and mobility. This advantage arises primarily from the continuous stretching and relaxation of elastomeric material that defines an active degree of freedom (DOF), prescribed during the manufacturing process. While the low elastic moduli of the soft material allows for infinite passive DOFs, each active DOF typically requires a valve and/or pump. On-board valving adds weight and size to the robots, and off-board valving requires tubing that imparts resistance to flow and requires higher pressure differentials for reasonable actuation velocities. In contrast to these methods, the work presented here exploits fluidic resistance in poroelastic foam actuators to create a traveling wave using only a single valve and pressure inlet. This concept is evaluated with respect to foam volume and fluid viscosity, and further demonstrated in a three-legged robot capable of millipede-inspired locomotion. The robot is capable of traveling at $\sim$1.1 mm/s, with individual legs (closest to the inlet) extending 41.28, 27.36, and 12.95 mm. These results represents an important step towards increasingly complex behavior in soft robots that remain simple to fabricate and control.**

I. INTRODUCTION

Soft actuators enable complex motion with inexpensive material, rapid manufacturing techniques, and low level control [1], [2]. When applied to full-scale robots however, these mechanisms typically require several chambers and separate pumps or many valves, as well as real time embedded control to produce useful behaviors. These add-ons increase price, complexity, weight, and rigidity of the robot. Here, we introduce the use of fluid resistance to produce wave-like actuation of a single chamber without the need for complex manufacturing, expensive materials and components, or accurate real-time control. An embodied control mechanism, determined by the soft actuator's shape, material properties, and internal fluid resistance, is used to produce consecutive movements along the length of the actuator from bursts of fluid created by simple on-off control of a single pump (Fig. 1). We demonstrate this concept through designs that produce forward locomotion with traveling wave patterns, much like those exhibited by a range of natural organisms from flatfish to millipedes [3].

A traveling wave provides the necessary forward momentum for an object by lifting subsequent regions of a linear body in successive fashion [4]. Traveling waves for locomotion have been reproduced with a range of techniques including FEAs [5], [6], shape memory alloys embedded into tubular meshworms [7], ionic polymer actuators embedded along beams [8], central pattern generators in (rigid) modular robots [9], and more. Furthermore, many other researchers have sought inspiration from locomotion in natural systems, including inchworms [10], caterpillars [11], fish [12], [13], jellyfish [14], and octopuses [15]. Similar to the minimalistic approach presented in this paper, researchers have demonstrated traveling wave locomotion using a single motor attached to a helix-shaped axle [16]. To the best of our knowledge, this is the first demonstration of locomotion by traveling waves in a soft robot, produced with only a single valve and pressure inlet.

In the following sections, we first describe design and fabrication of the poroelastic foam actuators (Sec. II). We then characterize the tensile strength of the foam and three different actuator designs with respect to the force exerted, the maximum deflection of the chamber, and the forward speed of the actuator along a flat surface (Sec. III). All three actuator designs have a spine-like structure with extruding segments, referred to as the ”legs”, along the length of the body. We show actuation with two fluids of different viscosity (air and water). Finally, we show simple locomotion by a robot with two sets of actuators coupled to a single source of pressure (Sec. IV) and conclude (Sec. V).

II. METHODS

To demonstrate the use of fluid resistance and traveling waves in soft actuators, we rely on FEAs and poroelastic foams. The following subsections briefly introduce the concept and fabrication of each.

A. Fluidic Elastomer Actuators

FEAs are a subset of soft actuators that use pressurization of elastomeric chambers to produce large deformations specific to localized strain patterns [1]. Strain-limiting layers on FEAs can be comprised of a wide set of materials, including inextensible fibers, fabric, or variable elastomer thicknesses, which upon pressurization of the FEA, produce a strain gradient, resulting in programmed bending or twisting of the elastomer [17].

FEAs with prismatic elastomer chambers are accurately manufactured with one- or two-step molding processes [2]; however, as the chamber shape becomes more complex, the number of fabrication steps also often increases and the repeatability of the final product often suffers. Recently, poroelastic foams were developed as a new class of FEAs

*This work was supported in part by the Cornell Sloan and Coleman Fellowship, and AFOSR Grant # FA9550-15-1-0160

[1]Sibley School of Mechanical and Aerospace Engineering, Cornell University, Ithaca, NY, USA ccf59@cornell.edu, sc2775@cornell.edu, rfs247@cornell.edu

[2]Materials Science and Engineering, Cornell University, Ithaca, NY, USA bcm79@cornell.edu

[3]Electrical and Computer Engineering, Cornell University, Ithaca, NY, USA kirstin@cornell.edu

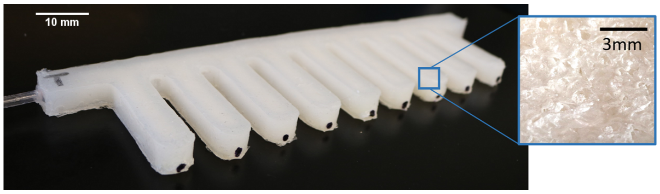

(a)

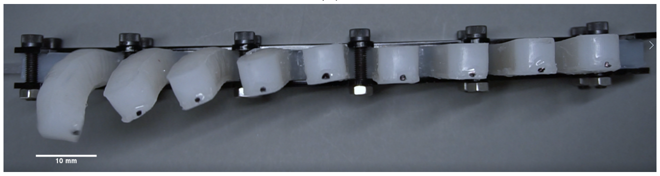

(b)

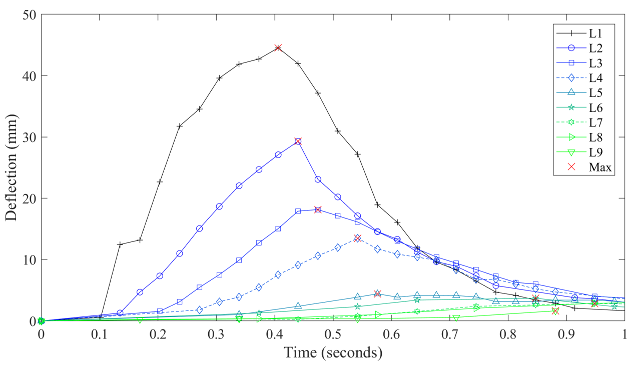

(c)

Fig. 1: Demonstration of how fluid resistance may be leveraged to create complex motions. (a) The experimental platform consists of a poroelastic foam actuator with a spine and nine legs; the inset shows a close-up of the internal foam. (b) Side view of the same actuator 0.15s after an air pressure of 20 psi has been applied. The higher deflection in the left-most extruding segment (closest to the inlet) demonstrates that fluid is retained closer to the inlet for a longer period of time. (c) Deflection of each leg (L1-9) over time when a pressure of 20 psi is applied for about 325 ms. At the end of the pulse, a valve is opened and the actuator returns to atmospheric pressure. Due to the geometric layout of the actuator, the legs closer to the inlet inflate more than the subsequent legs. The point of maximum deflection in each leg is marked in red. As this curve indicates, the resistance of the foam causes a damped traveling wave through the legs.

that offer greater complexity in soft, repeatable, smart 3D structures [17]. As opposed to elastomeric chambers where there is an internal volume of air, poroelastic foams contain minuscule, interconnected pockets of air spread throughout an elastomer. Pressurization of these actuators also results in programmed deformations; however, the period of time necessary for a foam chamber to reach pressure equilibrium across its volume drastically increases as a result of fluidic resistance which varies as a function of foam porosity, foam shape, and inflation pressure.

Fluidic resistance in poroelastic foams offers opportunities to design complex embodied control in soft robotic actuators, thus decreasing the need for external controllers. A traveling wave for instance can be created from multiple, neighboring chambers subsequently pressurized one right after the other; however, this requires external control and drivers to coordinate between the inflation and deflation of adjacent chambers. Instead, poroelastic foams offer an embodied control mechanism that can produce a traveling wave along the length of a single foam chamber.

B. Foam Fabrication

The poroelastic foams are fabricated with a lost- salt process, previously used in [17] and originally adapted from [18]. The matrix material is comprised of elastomer, and the porogen (the mass used to create the miniscule voids) comes from Himalayan salt. The foam is encapsulated into the spine-like Ecoflex 00-30 structure shown in Fig. 1a with 3, 5, and 9 legs respectively. The width of each leg is 16.26 mm; the gap between the legs are 93.73 mm, 38.86 mm, 11.43 mm respectively. In our design the foam serves two purposes. It enables an easy fabrication process as it automatically fills the void of the surrounding elastomer, and it provides added fluid resistance to create the traveling wave.

The fabrication process is split into two parts: foam sealing and strain sealing. All silicone used in this process was Ecoflex 00-30 (Smooth-On, Inc.), prepared as directed by the manufacturer. Other materials include: silicone adhesive (Silpoxy from Smooth-On, Inc.), non-woven nylon sheets (Soft n Sheer from Sulky of America), and Himalayan salt (Pure Himalayan Salt, 1-3mm). Table I shows the salt / Ecoflex 00-30 mixture ratios for the three actuators.

First, the foam is fabricated as indicated in Fig. 2A. The silicone and salt are mixed with corresponding mass amounts listed in Table 1, to reach 50.45% porosity, and cured in an acrylic laser cut mold at room temperature. The foam is then demolded and loosened by hand; the salt can be removed from dissolving in a sonicator or massaging the actuator by hand under running water.

Sealing the foam involves three steps (Fig. 2B). Layer 1 is cast using silicone and cured at room temperature. Layer 2

TABLE I: The actuators are fabricated using EcoFlex 00-30 (EF), Himalayan Salt (HS), and Silpoxy silicone adhesive. The different steps are described in Fig. 2. This table specifies the mixture of materials in grams.

Process	3 Legs	5 Legs	9 Legs
Foam Fabrication	29.95 g (HS) / 14.5 g (EF)	36.96 g (HS) / 17.9 g (EF)	50.8 g (HS) / 24.6 g (EF)
Layer 1	16 g (EF)	22 g (EF)	30 g (EF)
Foam-to-EF Adhesive Layer	8 g (EF)	8 g (EF)	11 g (EF)
Foam Sealing Layer	35 g	43 g	60 g
Strain Sealing Layer	50 g	75 g	95 g
Final Silpoxy Layer	5.2 g	6 g	9 g

(Foam-to-EF Adhesive Layer), is cast on top of Layer 1, with the desalted foam placed on top. This is cured in the oven (80^oC) to prevent the foam from soaking up an excessive amount of silicone and to allow it to become anchored to the first layer. This, in turn, prevents it from floating in the next step. The final layer (Foam Sealing Layer) seals the foam cavity; the silicone is poured on the foam and cured at room temperature. Any bubbles that form are popped manually.

The second part of the fabrication involves the strain-limiting layers for both the spine and the legs (Fig. 2C). These layers consist of a laser-cut non-woven nylon sheet to produce asymmetric bends upon inflation. Each leg and body is wrapped in an individual sheet, and attached to the sealed foam with silicone adhesive. To complete sealing of the strain-limiting layer to the sealed foam a final Strain Sealing Layer is casted. 50% of the layer's silicone is poured into the mold, and 40% is painted on all sides of the actuator. The painted actuator is placed top side down, and the last 10% of the silicone is poured on top of the mold. The mold is covered, weighted down, and allowed to cure in room temperature. Next, a 1/16" inlet tube is inserted 1" into the actuator, sealed with silicone adhesive, and cured in an oven at 80^oC for 10 minutes. Finally, a layer of silicone adhesive is added to the strained side of the mold and smoothed with a plastic (non-silicone) sheet. This is also allowed to cure in the oven at 80^oC for 20 minutes. Fig. 2D shows a side cross-sectional sketch of the assembled actuator.

III. ACTUATOR CHARACTERIZATION

To characterize the actuators, we first compare the tensile strength of the foam and the silicone. We then examine the relationship between actuator design and the traveling wave produced upon application of pressure. As previously stated we test three, five, and nine-legged actuators; the number of legs signify the number of locations at which the pressure within the actuator is temporally split two ways, causing differential pressure across the length of the actuator. Each of the three actuators was pressurized with air and water and characterized with respect to the exhibited deflection and speed of each leg. Force measurements for each leg were recorded when the actuator was inflated by air. Throughout the results, the first leg (L1) refers to the perpendicularly extruding segment closest to the inlet of the foam actuator. The last leg (L9) refers to the segment farthest away from the inlet.

As expected, throughout the results we observe that the viscosity of the fluid is strongly correlated with the fluid resistance, and therefore a critical parameter in the design of the traveling wave. We encourage the reader to view the accompanying video to view how a traveling wave behaves differently when the actuator is inflated with air and when it is inflated with water.

A. Tensile Test

Using a Zwick Roell z010 instrument, we conducted tensile tests on five pieces of Ecoflex 00-30 and five pieces of the Ecoflex 00-30 foam to demonstrate the differences in

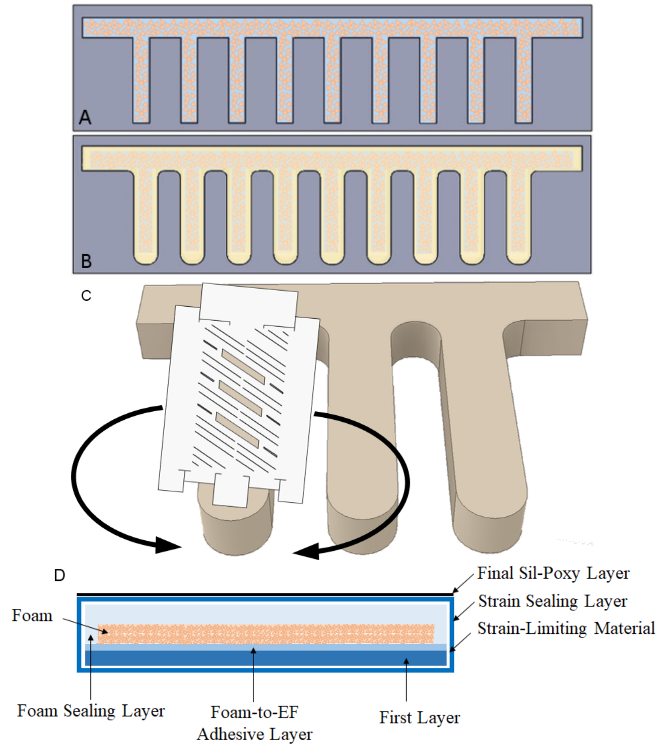

Fig. 2: Sketches showing the process to mold a 9-legged actuator. A) Mold of laser cut acrylic to cast the poroelastic foam. B) Foam-sealing layer, also molded in the acrylic mold. C) Strain-limiting layer wrapped around each finger along the body of the foam actuator. D) Side view of a complete foam actuator. The foam is sandwiched between equal layers of silicone to avoid bulging out on one side of the actuator. The strain-limiting layer is wrapped completely around the actuator, and a final layer of silicone adhesive is applied to one side of the actuator.

the material properties (Fig. 3). The foam is simply a porous medium of the Ecoflex 00-30 silicone, and as a result, the stiffness of the material is reduced by more than two times. The elastic modulus was found to be 50.894 ± 7.561 kPa for the Ecoflex and 19.805 ± 2.702 kPa for the foam. The strain of the two specimens is shown only up to 5 mm/mm, because the specimens started to slip at elongations greater than 600%. The tensile strength of Ecoflex is 1.379 MPa and the elongation at break is 900% [19]. These tests verify that the Ecoflex 00-30 has a higher stiffness than the poroelastic foam. The Ecoflex 00-30 therefore serves as a semi-rigid encasing structure for the foam to expand within. The foam must expand at a higher rate than the Ecoflex, so that the pores inside can be filled as air travels along the length of the actuator. At high pressures, the foam may stretch to its breaking point, and leave an empty space within the actuator where the fluid aggregates temporarily.

B. Actuator Force

We adopted a setup similar to that shown in Fig. 1b. A scale placed underneath the legs allowed us to measure the

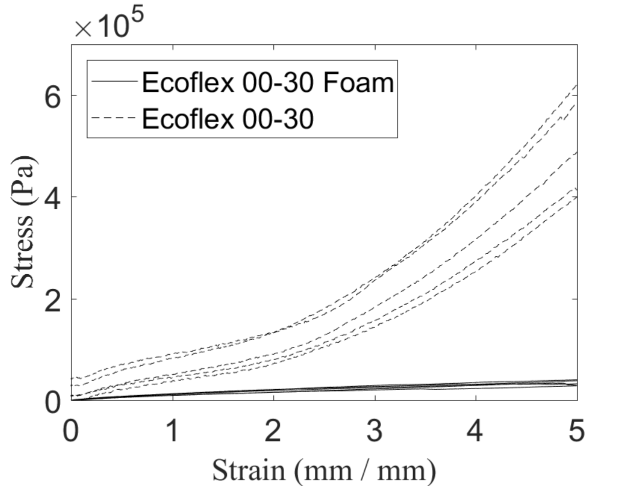

Fig. 3: Tensile tests conducted on Ecoflex 00-30 (Width = 14 ± 1 mm, Thickness = 1 mm) and Ecoflex 00-30 Foam (Width = 30 mm, Thickness = 5 mm ± 1 mm).

force exerted by each leg when pressurized by air. Table II shows the results of these tests. In the 3-legged actuator, the greatest amount of force produced by the first leg was 0.508±0.008 N, compared to 0.105±0.008 N by the last leg. Actuators with 5 and 9 legs have very small deflections at the last leg, below the resolution of our measurement techniques, and therefore are unlisted. We similarly tested the force application when the actuator was pressurized with water. However, due to the high viscosity of water, the legs expanded slowly and slipped over the scale of the actuator resulting in inaccurate data collection. Consequently, this data is not reported here.

C. Actuator Deflection

The individual leg deflection trajectory is controlled though a embedded custom strain layer. The strain layer is a non-woven nylon fabric cut to both wrap around the individual leg and direct the actuator's motion (Fig.1c). The strain layer was designed to produce bending and twisting, both necessary to achieve locomotion (Fig. 4). The angle of the slit controls twisting and the width of the slits control bending. These parameter can be further adjusted and tested to achieve faster locomotion.

The maximum vertical deflection of each leg in the three actuator designs is observed when inflated with air (Table III) and when inflated with water (Table IV). Figs. 1, 5, and 6 show that the maximum deflection of the legs exhibit an exponential decay as a function of the leg's distance from the inlet. Fluidic resistance causes a decrease in pressure in each consecutive leg, therefore over limited-time pressurization, the back legs do not experience the same maximum pressure as the legs closer to the inlet. The vertical deflection, a result of the pressure within the individual leg, decreases in each leg from the inlet.

TABLE II: Force exerted at maximum deflection by the legs closest and furthest from the inlet, when actuated by air at 20 psi. Essentially no force was exerted by the last leg in the 5- and 9- legged foam actuators. ($\overline{x} \pm \sigma_x; n = 4$).

Actuator	First Leg [N]	Last Leg [N]
3-Finger Actuator	0.508±0.008	0.105±0.008
5-Finger Actuator	0.432±0.012	-
9-Finger Actuator	0.434±0.029	-

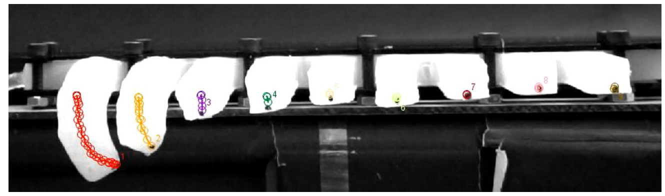

Fig. 4: The motion of the legs consist of bending and twisting, controlled by the design of an embedded custom strain layer

TABLE III: Maximum deflection, d_{max}, and velocity, v_{max}, exhibited by each leg in the three actuators when inflated with air at 20 psi. L1 refers to the extruded segment closest to the inlet and L9 refers to the extruded segment farthest away from the inlet.

Leg no.	3		5		9	
	d_{max} [mm]	v_{max} [mm/s]	d_{max} [mm]	v_{max} [mm/s]	d_{max} [mm]	v_{max} [mm/s]
L1	41.28	563.22	49.00	363.73	40.69	352.35
L2	-	-	-	-	29.03	195.1
L3	-	-	25.45	128.42	18.14	84.18
L4	-	-	-	-	13.46	61.21
L5	27.36	140.06	22.23	125.88	4.42	22.96
L6	-	-	-	-	3.63	10.52
L7	-	-	9.58	52.00	2.87	9.19
L8	-	-	-	-	3.63	6.12
L9	12.95	72.49	6.30	42.88	1.57	7.65

Discrepancies in the decay of the maximum vertical deflection for the 5-legged actuator is due in part to imperfections in the fabrication procedure. A difference in the layer thickness of the Ecoflex in any of the steps described in Sec. II-B can result in slightly higher straining on one side. At higher pressures, these imperfections can cause rips in the Ecoflex, rendering the actuator useless.

Notice also how the number of legs correlates with the time it takes legs further from the inlet to equalize to ambient pressure. In the 9-legged actuator all legs return to 0mm deflection in one second, shown in Fig. 1c; whereas the legs further from the inlet take longer to equalize pressure when more legs are present (Figs. 5 and 6). Again, this is due to the fact that the designs with less legs reached higher pressures within the 325ms applied pulse.

IV. ROBOT DEMONSTRATION

To demonstrate proof-of-concept locomotion, we added two 3-legged actuators to either side of a rigid backbone. We do not show locomotion with 5-and 9-legged actuators since only very minor forward locomotion is exhibited due in part to increased actuator weight and in part to exponentially

TABLE IV: Maximum deflection, d_{max}, and velocity, v_{max}, exhibited by each leg in the three actuators when inflated with water at 3.24 ± 0.12 mL/s. L1 refers to the extruded segment closest to the inlet and L9 refers to the extruded segment farthest away from the inlet.

Leg no.	3		5		9	
	d_{max} [mm]	v_{max} [mm/s]	d_{max} [mm]	v_{max} [mm/s]	d_{max} [mm]	v_{max} [mm/s]
L1	34.01	22.96	35.26	14.287	32.61	17.91
L2	-	-	-	-	28.68	12.98
L3	-	-	20.84	3.90	24.46	3.81
L4	-	-	-	-	22.81	3.43
L5	16.56	5.64	17.191	3.33	21.18	2.31
L6	-	-	-	-	21.18	2.13
L7	-	-	18.74	2.49	17.91	1.50
L8	-	-	-	-	18.26	1.83
L9	23.57	7.98	17.86	1.25	18.59	1.80

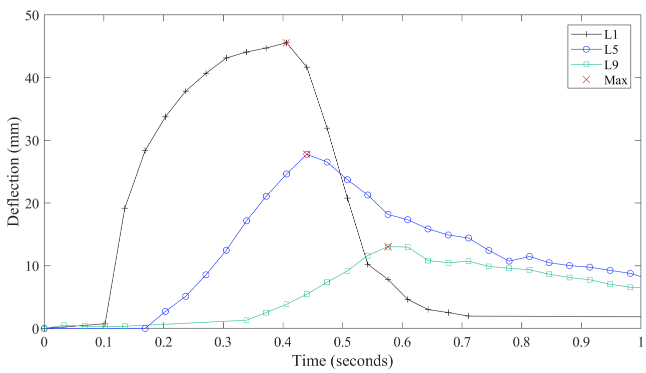

Fig. 5: 3 legs, traveling wave.

decaying deflections. The 3-legged actuator were coupled through 1/16" tubes and pressurized with air through a pump at 16.5 psi. Each pulse of air lasts 325ms, separated by 1000ms deflation cycles. In this experiment the robot travels 39 mm over 6 min (Fig. 7). The traveling wave creates a frictional contact differential throughout the length of the actuators, allowing them to crawl forward (Fig. 8). Observe in Figure 5, how the leg closest to the inlet first exhibits maximum deflection (0.4s), bending down and backwards to drag the hind body along; then as the front leg deflates, the hind leg achieves maximum deflection (0.58s) which causes enough friction to keep the front stationary.

To test whether the motion was indeed caused by the traveling wave, and not just the asymmetric strain limiting layers incorporated into the legs, we created a separate actuator in which the foam was replaced with an empty chamber. In this version, all legs inflated simultaneously and by the same amount due to the negligible fluid resistance. Over five inflation/deflation cycles the robot did not produce any forward locomotion, compared to 7.3mm that the robot with foam walked.

Furthermore, we examined how much the inflation of the hind legs aid the locomotion speed of the robot. To do this, we added a zip tie around the actuator just after the first legs, cutting off all other legs from pressurization. This in turn means that the majority of the actuator remains limp

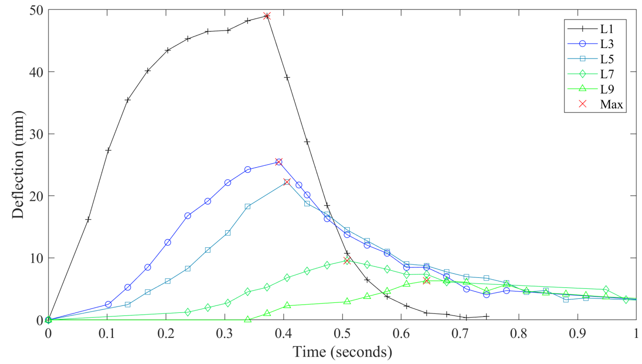

Fig. 6: 5 legs, traveling wave.

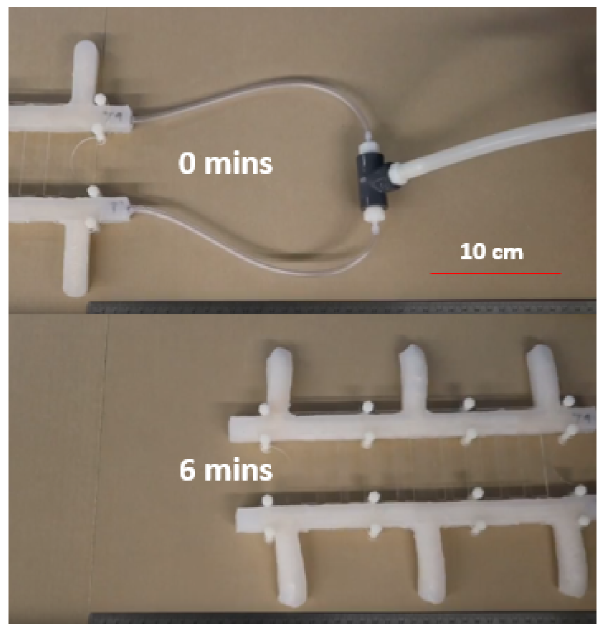

Fig. 7: Two soft robotic actuators attached to a rigid backbone crawl forward at a rate of approximately 1.1 mm/s for a period of six minutes.

while the first legs provide force to move the robot forward. When inflated at 8 psi, the actuator moves forward a distance of 15 cm over three minutes, resulting in a velocity of approximately 0.83 mm/s. By comparing this number to the locomotion of the full robot (1.1 mm/s), we see that the last four legs increase the speed by 32.5%.

It should be noted that the undisturbed 3-legged actuators were inflated at 16.5 psi; however, due to foam resistance and splitting of the airway between the spine and the first leg, it can be assumed that at the beginning of the pulse the first leg is actually pressurized at 8.25 psi, half the inlet pressure. A number of parameters can be adjusted to improve the robot's locomotive speed including foam porosity, number of legs, and material strain. Another set of variables that can be optimized are the inflation cycle parameters (i.e. pressure, inflation time, deflation time). It should be noted that a careful combination of these parameters is necessary

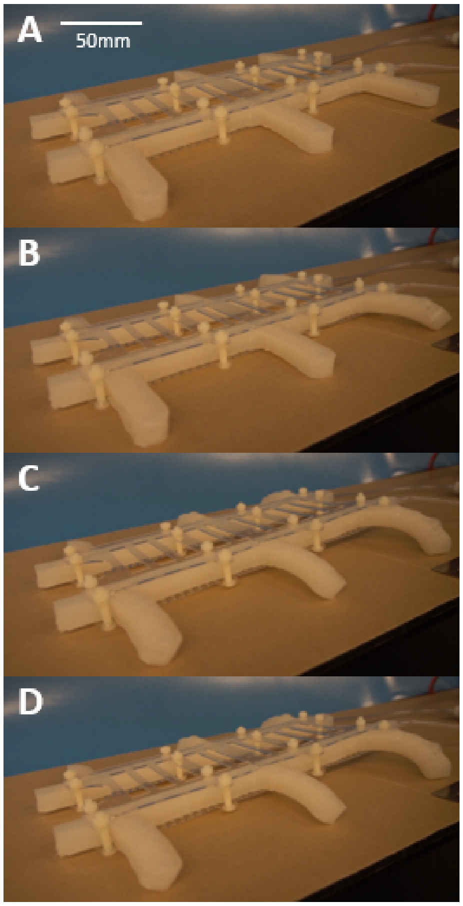

Fig. 8: The undulating wave in four steps: A) $t = 0$. There is no actuation in any of the legs. B) $t = 166.7\ ms$. L1 is approaching peak actuation. C) $t = 333.3\ ms$. L1 is at peak actuation, L5 is approaching peak actuation, and L9 is starting to actuate. D) $t = 466.7\ ms$. L1 is approaching zero actuation, L5 is post peak actuation, L9 is at peak actuation.

to avoid failure from the build up of high pressures within the actuator.

V. CONCLUSIONS

Many robotic implementations can benefit from reduced complexity. Here, we have shown that poroelastic foams may be useful in reducing the number of additional components (pumps, valves, embedded controllers) necessary to produce intricate motions. Fluid resistance in the foams is exploited to produce traveling waves, even though only a single inlet pressure is applied to the actuator.

The determining factors in the flow rate of a fluid throughout the length of the foam include foam shape, foam porosity, number of extruding sections of foam, the inlet pressure, and fluid viscosity. In this paper we examined the effect of the volume of foam and the fluid viscosity. The optimal settings for the remaining parameters were manually estimated. We showed that with careful design considerations, it is possible to produce repeatable traveling wave motions along the length of the actuator. The length of the spine as well as position and number of extruding legs determine the velocity of the traveling wave, the maximum deflection and force exerted by individual legs, and, as a result, the forward velocity of the robot when used for locomotion.

The embodied control methodology proposed lends itself to a great variety of future applications. Next, we intend to focus on simpler fabrication methods and validated models to further enhance the design of embodied intelligent soft robots that can exhibit complex motions with simple drivers and control.

REFERENCES

[1] D. Rus and M. T. Tolley, Design, fabrication and control of soft robots, Nature, vol. 521, no. 7553, pp. 467475, 2015.

[2] L. Hines, K. Petersen, G. Z. Lum, and M. Sitti, Soft Actuators for Small-Scale Robotics, Adv. Mater., vol. 29, no. 13, 2017.

[3] S. Grillner, "Control of locomotion in bipeds, tetrapods, and fish." Comprehensive Physiology, 2011.

[4] X. Zhou, C. Majidi, and O. M. OReilly, Flexing into motion: A locomotion mechanism for soft robots, Int. J. Non. Linear. Mech., vol. 74, pp. 717, 2015.

[5] C. D. Onal and D. Rus, Autonomous undulatory serpentine locomotion utilizing body dynamics of a fluidic soft robot, Bioinspiration and Biomimetics, vol. 8, no. 2, 2013.

[6] Y. Nakazato, Y. Sonobe, and S. Toyama, Development of an In-pipe micro mobile robot using peristalsis motion, J. Mech. Sci. Technol., vol. 24, no. 1, pp. 5154, 2010.

[7] S. Seok, C. D. Onal, K.-J. Cho, R. J. Wood, D. Rus, and S. Kim, Meshworm: a peristaltic soft robot with antagonistic nickel titanium coil actuators, IEEE/ASME Trans. mechatronics, vol. 18, no. 5, pp. 14851497, 2013.

[8] K. Takagi, M. Yamamura, Z.-W. Luo, M. Onishi, S. Hirano, K. Asaka, and Y. Hayakawa. "Development of a rajiform swimming robot using ionic polymer artificial muscles." In Intelligent Robots and Systems, 2006 IEEE/RSJ International Conference on, pp. 1861-1866. IEEE, 2006.

[9] J. Conradt and P. Varshavskaya. "Distributed central pattern generator control for a serpentine robot." In Proceedings of the International Conference on Artificial Neural Networks (ICANN), pp. 338-341. 2003.

[10] W. Wang, J.-Y. Lee, H. Rodrigue, S.-H. Song, W.-S. Chu, and S.-H. Ahn, Locomotion of inchworm-inspired robot made of smart soft composite (SSC), Bioinspir. Biomim., vol. 9, no. 4, p. 46006, 2014.

[11] H.-T. Lin, G. G. Leisk, and B. Trimmer, GoQBot: a caterpillar-inspired soft-bodied rolling robot, Bioinspir. Biomim., vol. 6, no. 2, p. 26007, 2011.

[12] H. El Daou, T. Salume, L. D. Chambers, W. M. Megill, and M. Kruusmaa, Modelling of a biologically inspired robotic fish driven by compliant parts, Bioinspiration and Biomimetics, vol. 9, no. 1, 2014.

[13] A. D. Marchese, C. D. Onal, and D. Rus, Autonomous Soft Robotic Fish Capable of Escape Maneuvers Using Fluidic Elastomer Actuators, Soft Robot., vol. 1, no. 1, pp. 7587, 2014.

[14] J. C. Nawroth, H. Lee, A. W. Feinberg, C. M. Ripplinger, and L. Megan, A tissue-engineered jellyfish with biomimetic propulsion.pdf, vol. 30, no. 8, pp. 792797, 2014.

[15] R. V. Martinez et al., Robotic tentacles with three-dimensional mobility based on flexible elastomers, Adv. Mater., vol. 25, no. 2, pp. 205212, 2013.

[16] Zarrouk, David, Moshe Mann, Nir Degani, Tal Yehuda, Nissan Jarbi, and Amotz Hess. "Single actuator wave-like robot (SAW): design, modeling, and experiments." Bioinspiration & biomimetics 11, no. 4 (2016): 046004.

[17] B. C. Mac Murray et al., Poroelastic Foams for Simple Fabrication of Complex Soft Robots, Adv. Mater., vol. 27, no. 41, pp. 63346340, 2015.

[18] H. R. Lin, C. J. Kuo, C. Y. Yang, S. Y. Shaw, and Y. J. Wu, Preparation of macroporous biodegradable PLGA scaffolds for cell attachment with the use of mixed salts as porogen additives, J. Biomed. Mater. Res., vol. 63, no. 3, pp. 271279, 2002.

[19] Smooth - on, Ecoflex® Series, 2011.